INORGANIC CHEMISTRY FRONTIERS

RESEARCH ARTICLE

View Article Online
View Journal

Cite this: DOI: 10.1039/d6qi00548a

Titanium-mediated coupling of CO_2 and ethylene to form acrylate: mechanistic insights from Cp^*_2Ti complexes

Areum Kim, [a] Nayeong Seok, [b] Mijung Lee, [c] Young Kyu Hwang, [c] Jeongcheol Shin *[d] and Changho Yoo *[a,b]

The coupling of CO_2 and ethylene to form acrylate is a promising route for CO_2 utilization, yet known catalytic systems are limited by low activity and harsh reaction conditions. These limitations are closely linked to the difficulty of metallalactone intermediate formation in late transition metal systems. Here, we investigate titanium-mediated coupling of CO_2 and ethylene to form acrylate using Cp^*_2Ti complexes and elucidate the elementary steps that enable acrylate formation under mild conditions. The oxophilic titanium promotes CO_2/ethylene coupling with a low activation barrier, and the resulting Ti(IV) metallalactone is thermodynamically stabilized by strong Ti–O interactions. Subsequent conversion to acrylate is readily achieved through deprotonation by an alkoxide base, while the canonical β-hydride elimination pathway remains unfavorable. Despite the kinetic accessibility of acrylate formation, mechanistic studies reveal that catalytic turnover is limited by competing Ti(II)/Ti(IV) comproportionation. These findings outline the operative steps and current limitations of titanium-mediated acrylate synthesis and provide a basis for the design of early transition metal catalysts for carboxylation chemistry.

Received 24th March 2026,
Accepted 30th April 2026

DOI: 10.1039/d6qi00548a

rsc.li/frontiers-inorganic

Introduction

CO_2 utilization has emerged as a key strategy for mitigating environmental threats and harnessing it as a sustainable carbon source.[1–4] Among various approaches, carboxylation using CO_2 is attractive, as organic carboxylic acids find widespread use in the chemical industry.[5–7] In particular, acrylic acid is an important feedstock for polymers, coatings, adhesives and absorbent materials.[8–12] Since the first Ni-catalyzed synthesis of acrylate from CO_2 and ethylene in 2012,[13] research has predominantly focused on Ni and Pd systems, exploring various ligands, bases, solvents, and additives (Fig. 1A).[9–24] Despite notable progress, catalytic systems still exhibit limited activity and require harsh conditions, with the best reported performance corresponding to 570 turnovers at 140 °C and 30 bar.[24] These limitations are attributed to slow kinetics rather than catalyst deactivation or side reactions.[20,25] Recent studies have extended to group 8 and 9 metals,[26–32] yet these have not overcome such limitations, motivating exploration of alternative metals beyond late transition metals.

A fundamental challenge in developing efficient carboxylation catalysts lies in the formation of a metallalactone intermediate *via* oxidative coupling of ethylene and CO_2, which is both kinetically and thermodynamically demanding (Fig. 1B).[13,25,33–35] In d^{10} late metals such as Ni^0 and Pd^0 complexes, fully occupied d orbitals disfavor CO_2 coordination, leading to high-energy transition states for coupling between ethylene and CO_2. This intrinsic electronic property accounts for the harsh conditions required for Ni and Pd catalysts. In contrast, early transition metals may present distinct opportunities. Their vacant d orbitals can facilitate CO_2 binding, lowering the kinetic barrier to metallalactone formation (Fig. 1B). In addition, the oxophilic Ti^{IV} forms strong Ti–O bonds, enhancing the thermodynamic stability of metallalactone species (Fig. 1B).

Literature precedents have shown that early transition metals can indeed form metallalactone species.[36–42] However, prior studies primarily focused on their synthesis, while their formation energetics and acrylate-relevant reactivity remain underexplored. Among early transition metals, titanium stands out as an appealing platform owing to its strong oxophilicity and versatile redox behaviour, which enable diverse chemistry in small-molecule activation and cross-coupling reactions,[43–46] suggesting its potential to mediate carboxylation chemistry.

[a]Department of Chemistry, Ulsan National Institute of Science and Technology (UNIST), Ulsan 44919, Republic of Korea. E-mail: cyoo@unist.ac.kr
[b]Graduate School of Carbon Neutrality, Ulsan National Institute of Science and Technology (UNIST), Ulsan 44919, Republic of Korea
[c]Green Carbon Research Center, Korea Research Institute of Chemical Technology, Daejeon 34114, Republic of Korea
[d]Department of Chemistry, Duksung Women's University, Seoul 01369, Republic of Korea. E-mail: jcshin91@duksung.ac.kr

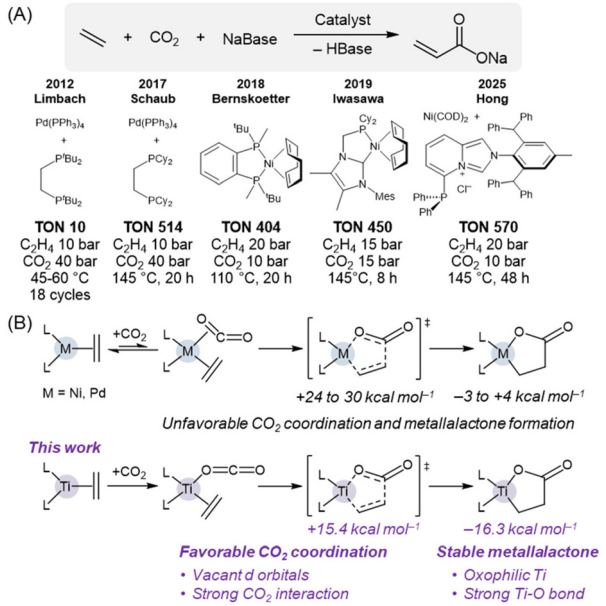

Fig. 1 (A) Representative catalysts for the coupling of ethylene and CO_2 to form acrylate. (B) Conceptual comparison of the metallalactone formation pathway for group 10 metals (Ni, Pd) and titanium. Free energies for Ni/Pd systems are taken from ref. 13, 25, 33–35.

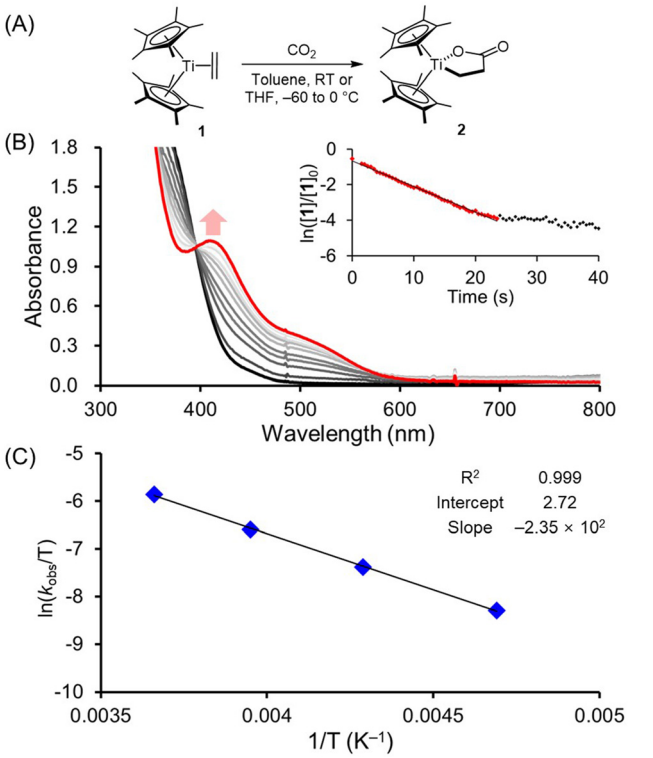

Fig. 2 (A) Reaction of **1** with CO_2 to form **2**. (B) UV-Vis spectral changes from **1** (black) to **2** (red) in THF at –40 °C. The inset shows the absorbance at 410 nm. (C) Eyring plots constructed using k_{obs} values measured at 0, –20, –40 and –60 °C.

In this study, we investigate titanium-mediated coupling of ethylene and CO_2 to form titanalactone and its reactivity toward acrylate synthesis. Using Cp^*_2Ti complexes, we elucidate the kinetic and thermodynamic landscape of elementary steps and competing pathways, and identify the factors limiting catalytic turnover, thereby providing a mechanistic insight into titanium-mediated ethylene carboxylation.

Results and discussion

Kinetic and thermodynamic analysis of titanalactone formation

Earlier reports have described the formation of metallalactone complexes across several early transition metals, including Ti,[36] V,[37] Zr,[38] Mo,[39–41] and W.[39,40,42] These reports demonstrate that early transition metals are capable of mediating the coupling of ethylene and CO_2 under stoichiometric conditions. However, the kinetic and thermodynamic aspects of metallalactone formation and its reactivity toward acrylate production have not been examined. Among the reported systems, the titanalactone is particularly notable, as it can be generated at low temperature,[36] suggesting relatively favorable kinetics. This compound was first reported in 1985 by Cohen and Bercaw, who observed the reaction of $Cp^*_2Ti(C_2H_4)$ (**1**) with 1 equiv. of CO_2 at −78 °C to afford $Cp^*_2Ti(C_2H_4CO_2)$ (**2**).[36] We therefore first revisited the formation of **2**.

Addition of CO_2 (50 equiv.) to **1** in toluene at room temperature resulted in an immediate color change from green to red (Fig. 2A). Product **2** was isolated in 85% yield and identified by its characteristic ^{1}H NMR triplets at δ 3.41 and 1.14 ($^3J_{HH}$ = 7.9 Hz). Given the rapid reaction at room temperature, the kinetics of formation of **2** were monitored at low temperatures by UV-Vis spectroscopy (Fig. 2B). Upon exposure of **1** to CO_2 (50 equiv.) at 0 °C, complete conversion was achieved within minutes, with an observed rate constant (k_{obs}) of 0.78 s^{-1}. Eyring analysis across the temperature range from −60 to 0 °C afforded a low activation enthalpy ($\Delta H^{\ddagger}_{298K}$= +4.7 kcal mol^{-1}) and a free energy of $\Delta G^{\ddagger}_{298K}$ = +15.3–17.1 kcal mol^{-1} (Fig. 2C and S19). The range arises from the uncertainty in the concentration of dissolved CO_2 under the reaction conditions, with the upper bound (+17.1 kcal mol^{-1}) corresponding to the apparent value from Eyring analysis without entropy correction, while the lower bound (+15.3 kcal mol^{-1}) was obtained by applying the maximum entropic correction ($T\Delta S$ = 1.8 kcal mol^{-1}) under the assumption of complete CO_2 dissolution. The DFT-computed barrier of +15.4 kcal mol^{-1} (*vide infra*, Fig. 4A, Path a) falls within this experimentally bracketed range, supporting a low kinetic barrier for C_2H_4–CO_2 coupling at a titanium center. Notably, this rate places the Ti system in a fundamentally different kinetic regime from late transition metal analogues. Ni and Pd systems exhibit hour-scale metallalactone formation kinetics.[13,22,25] Consistent with these slow kinetics, DFT studies have proposed activation barriers on the order of ~30 kcal mol^{-1} for metallalactone formation at nickel and palladium centers.[13,25,33–35] These results show that metallalactone formation at the titanium center is an exceptionally

fast process, in contrast to Ni and Pd systems, where this step is often kinetically limiting.

Compound **2** remained robust upon isolation, showing no indication of decarboxylation back to **1** over several weeks. The crystal structure of **2** provides insight into its stability (Fig. 3A and Table 1). The Ti–O bond (2.016(4) Å) is 0.133 Å shorter than the Ti–C bond (2.149(5) Å), whereas the analogous Pd and Ni complexes exhibit smaller M–O/M–C differences (Δd = −0.008 Å for Pd and −0.050 Å for Ni).[17,22] This pronounced Ti–O contraction reflects strong oxophilicity of titanium. The density functional theory (DFT)-optimized geometry of **2** also reproduces this structural feature, with Ti–O and Ti–C bond lengths of 1.964 and 2.223 Å, respectively. Wiberg bond index analysis further indicates that both the Ti–O and Ti–C interactions in **2** are stronger than the corresponding bonds in the Ni analogue, reflecting strong covalent interactions in the Ti complex, with a particularly large difference for the M–O interaction (0.557 for Ti *vs.* 0.276 for Ni). Natural population analysis reveals a more electropositive metal center in the Ti complex compared with the Ni congener, consistent with a more strongly polarized metal–oxygen interaction. These analyses are consistent with the pronounced oxophilicity of titanium and strong Ti–O interaction, providing thermodynamic stabilization to the metallalactone framework in **2**.

Computed energy profiles support the advantage of titanium in metallalactone formation relative to Ni and Pd systems. Oxidative coupling between **1** and CO_2 proceeds *via* a five-membered transition state, which is strongly exergonic (ΔG = −16.3 kcal mol^{-1}) with a low activation barrier ($\Delta G^{\ddagger}$ = +15.4 kcal mol^{-1}) under standard conditions (Fig. 4A, Path a). No stable CO_2-bound intermediate is found along the reaction coordinate; instead, CO_2 coordination directly leads to the titanalactone product. In contrast, CO_2 binding to Ni(NHC-P)(C_2H_4) is unfavorable (ΔG = +4.4 kcal mol^{-1}), and the product formation is only slightly exergonic (ΔG = −3.7 kcal mol^{-1}, Table S5), with a higher barrier ($\Delta G^{\ddagger}$ = +17.9 kcal mol^{-1}, Table S5). The Pd(dmpe) analogue also shows unfavorable CO_2 binding (ΔG = +8.5 kcal mol^{-1}), slightly endergonic palladalactone formation (ΔG = +0.4 kcal mol^{-1}), and a substantially higher barrier ($\Delta G^{\ddagger}$ = +24.4 kcal mol^{-1}, Table S6).

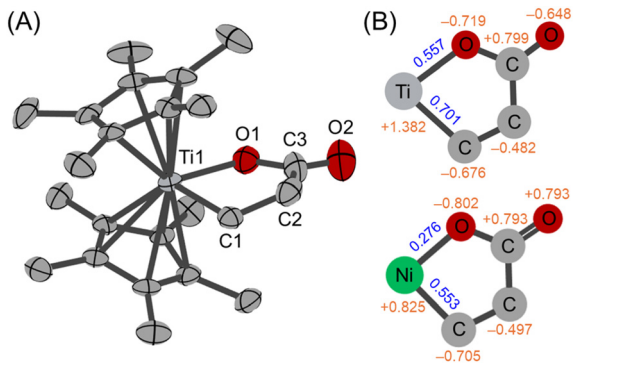

Fig. 3 (A) Structural representation of **2** with ellipsoids shown at 50% probability. (B) Wiberg bond indices (blue) and natural population analysis charges (orange) for the metallalactone fragment of compound **2** and (NHC-P)Ni($C_2H_4CO_2$).

Table 1 Comparison of bond distances and orders in metallalactone compounds

	Ti	Ni
Bond distances[a]		
d_{M-O} (Å)	2.016(4)	1.880(3)
d_{M-C} (Å)	2.149(5)	1.930(7)
Δd[b] (Å)	−0.133	−0.050
Wiberg bond indices[c]		
M–O	0.557	0.276
M–C	0.701	0.553
Natural population analysis charges[c]		
M	+1.382	+0.825
O	−0.719	−0.802
C	−0.676	−0.705

[a] Distances from X-ray diffraction data; values for the Ni compound are taken from ref. 22. [b] Difference between d_{M-O} and d_{M-C}. $\Delta d = d_{M-O} - d_{M-C}$. [c] Wiberg bond indices and NPA charges for both compounds were computed at the TPSS/6-311g(d,p) level of theory.

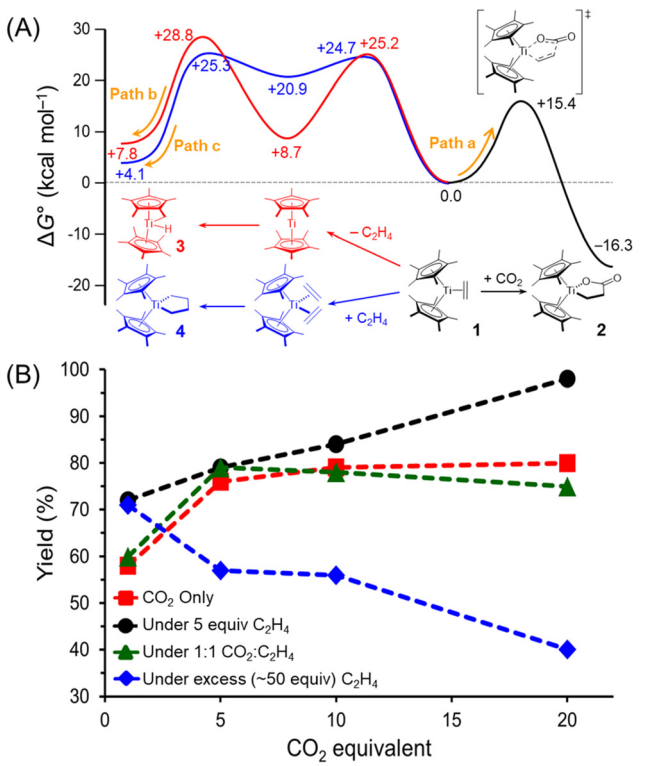

Fig. 4 (A) Calculated free energies for titanalactone (Path a, black), ethylene dissociation followed by Cp* C–H activation (Path b, red) and ethylene cyclization (Path c, blue). (B) Yield of **2** with varying amounts of CO_2 and C_2H_4.

Computational results are consistent with the experimentally observed reactivity. The corresponding Ni and Pd systems require harsh conditions to shift the equilibrium and overcome slow kinetics,[22,25] whereas the titanium system enables thermodynamically favorable metallalactone formation with a low kinetic barrier.

Stoichiometric effects on titanalactone formation

Although the formation of titanalactone **2** proceeds efficiently, the conversion is not quantitative under stoichiometric conditions, indicating the presence of competing pathways. To identify side reactions that limit lactone formation, the conversion of **1** to **2** was monitored by ^{1}H NMR spectroscopy. CO_2 addition to **1** led to the disappearance of **1** and the formation of **2** along with free C_2H_4 (δ 5.25), indicating the partial dissociation of C_2H_4 from **1** (Fig. S21). Low-intensity aliphatic signals (δ 0.8–2.0) also appeared, one matching the known Cp* C–H activation product **3** (Fig. S21).[47] These indicate that ethylene dissociation from **1** and subsequent C–H activation occur in parallel with the productive CO_2 insertion pathway.

To minimize side reactions associated with C_2H_4 dissociation, the effects of CO_2 and C_2H_4 equivalents on the yield of **2** were investigated (Fig. 4B). Reaction of **1** with 1 equiv. of CO_2 gave **2** in 60% yield, which gradually increased to 85% with higher CO_2 loading. Notably, the addition of a small amount of ethylene (5 equiv.) improved the yield to 98%, consistent with suppression of ethylene dissociation. In contrast, excess ethylene (~50 equiv.) led to a decrease in the yield of **2**, presumably due to the formation of the titanacyclopentane species $Cp^*_2Ti(C_4H_8)$ (**4**).[48] Compound **1** can form **4** in equilibrium under C_2H_4,[48] and therefore, excess C_2H_4 shifts the equilibrium toward **4** and hinders the formation of **2**.

DFT calculations support the experimentally observed energy relationships for lactone formation and side reactions (Fig. 4A). Ethylene dissociation from **1** generates Cp^*_2Ti, which can subsequently undergo C–H activation of the Cp* ligand (Fig. 4A, Path b).[47] The formation of the S = 1 decamethyltitanocene is endergonic (ΔG = +7.8 kcal mol^{-1}), while the corresponding S = 0 excited state lies 9.6 kcal mol^{-1} higher, consistent with its experimentally observed paramagnetic nature.[47] The ethylene dissociation and subsequent C–H activation proceed with the overall barrier reaching $\Delta G^{\ddagger}$ = +28.8 kcal mol^{-1}. Alternatively, coordination of an additional C_2H_4 can initiate cyclization to form **4** (Fig. 4A, Path c).[48] This process is slightly endergonic (ΔG = +4.1 kcal mol^{-1}) and proceeds through a moderate activation barrier ($\Delta G^{\ddagger}$ = +25.3 kcal mol^{-1}), in reasonable agreement with the experimentally determined thermodynamics.[48] Taken together, both pathways may be energetically accessible under CO_2-deficient conditions but are expected to be kinetically suppressed in a CO_2-rich environment. While low C_2H_4 loading prevents C_2H_4 dissociation from **1**, under C_2H_4-rich conditions, **1** can be predominantly converted to **4**, suppressing productive titanalactone formation. Careful control of both substrates is therefore important to maximize the yield of **2** while minimizing competing side products.

Reactivity of titanalactone toward acrylate formation

The reactivity of titanalactone species **2** toward acrylate formation was investigated through potential β-hydride elimination or direct deprotonation pathways (Fig. 5).[13,34,49] β-Hydride elimination from metallalactones requires prior ring opening to adopt a geometry in which the β-hydrogen is positioned *syn*-coplanar with the metal center. This conformational rearrangement incurs a significant energetic penalty (Fig. 5A).[33,50] In the case of titanium, this pathway is expected to be even more challenging due to the robust Ti–O interaction and the d^0 electronic configuration of the titanium center. Indeed, thermolysis of **2** up to 150 °C resulted only in decomposition without any detectable acrylate formation.

To further evaluate whether β-hydride elimination could be accessible, we explored the effect of electrophiles, inspired by previous studies on nickel and palladalactone systems in which an electrophile promotes M–O bond cleavage and subsequent β-hydride elimination.[50–54] Although the addition of $NaBAr^F_4$ or MeI to **2** did not result in any observable elimination or speciation, treatment with the stronger electrophile MeOTf led to *O*-methylation to afford the cationic methylated lactone complex $[Cp^*_2Ti(C_2H_4CO_2Me)][OTf]$ (**5**) (Fig. 5B). Compound **5** retains the characteristic lactone triplets at δ 3.25 and 1.42 ($^3J_{HH}$ = 7.84 Hz) in the ^{1}H NMR spectrum, along with new methyl resonances observed at δ 3.88 in ^{1}H NMR and at δ 57.28 in the ^{13}C NMR spectra. The solid-state structure of **5** confirms methylation at the distal oxygen atom and reveals a slightly elongated yet persistent Ti–O interaction (average Ti–O = 2.083 Å in **5** *vs.* 2.016(4) Å in **2**) (Fig. 6A). Although the *O*-methylation formally neutralizes the anionic oxygen in the carboxylate moiety and would be expected to promote Ti–O bond cleavage, the retention of Ti–O interaction shows the

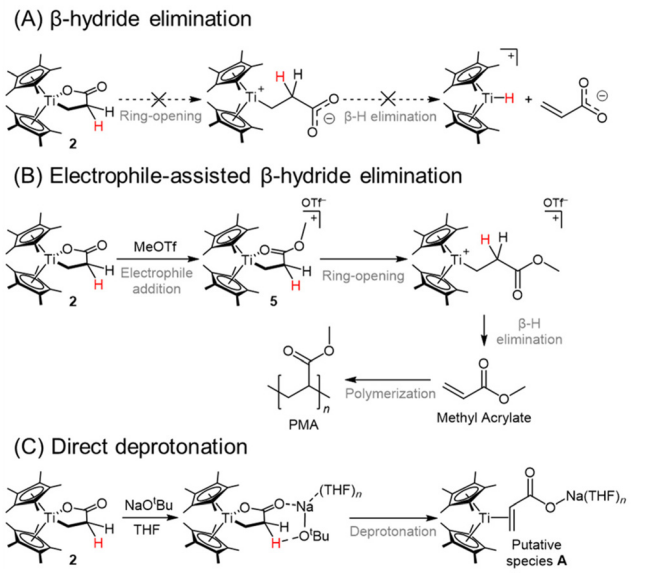

Fig. 5 Conversion of metallalactone to acrylate *via* (A) β-hydride elimination, (B) electrophile-assisted β-hydride elimination, and (C) direct deprotonation.

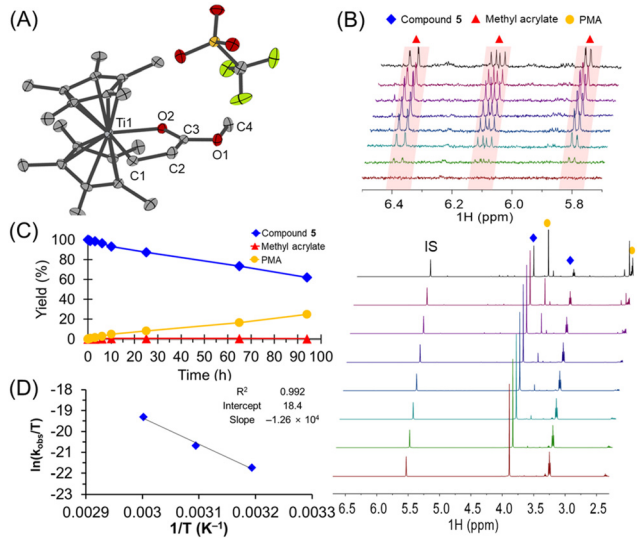

Fig. 6 (A) Structural representation of **5**. (B) ^{1}H NMR spectra showing methyl acrylate and PMA formation from **5**. (C) The concentration changes of **5**, methyl acrylate and PMA. (D) Eyring plots constructed using k_{obs} values measured at 40, 50 and 60 °C.

strong oxophilicity of the titanium center. Consistent with this structural observation, the IR spectrum of **5** exhibits a red-shifted carbonyl stretching frequency at 1612 cm^{-1} relative to **2** (1670 cm^{-1}), which reflects weakening of the C=O bond upon electron donation to the titanium center and supports the presence of Ti–O interaction even after neutralization of the carboxylate.

A trace amount of methyl acrylate was detected in the NMR spectrum of **5**, indicating that β-hydride elimination from **5** is accessible (Fig. 6B). Upon heating **5** at 60 °C, however, only a small amount (0.5%) of methyl acrylate accumulated over 24 h, and the yield did not increase further. Instead, formation of poly(methyl acrylate) (PMA) was observed (Fig. 6B), demonstrating that the produced methyl acrylate is consumed more rapidly by polymerization than it is formed. As a result, methyl acrylate remains at a low steady-state concentration (0.5%), and **5** follows pseudo-first-order decay. The conversion of **5** is slow, with a k_{obs} of 1.4 × 10^{-6} s^{-1} at 60 °C (Fig. 6C). Eyring analysis over the range of 40–60 °C affords a high activation barrier ($\Delta G^{\ddagger}$) of +28.2 kcal mol^{-1} (Fig. S28). These results indicate that the promotional effect of the electrophile on β-hydride elimination is limited in titanium, which contrasts with the Ni system, where MeOTf readily cleaves the Ni–O bond and releases methyl acrylate in high yield.[52] Although methylation weakens the Ti–O bond, the residual Ti–O coordination may remain sufficiently strong to disfavor β-hydride elimination.

To circumvent the intrinsic limitations associated with β-hydride elimination in the titanalactone system, a direct deprotonation pathway was explored as an alternative strategy for acrylate formation (Fig. 5C). Treating **2** with 1 equiv. of NaO^{t}Bu in THF resulted in a rapid color change from orange to dark green within 30 min. The ^{1}H NMR spectrum showed complete disappearance of lactone signals, accompanied by the appearance of broad resonances in the acrylate region (δ 4.8–6.2). Although the putative Ti^{II}–acrylate species **A** could not be isolated, its transient formation is supported by D_2O quenching experiments, which afforded the free sodium acrylate product in 24% yield. A series of bases with varying basicity were evaluated (Table 2). Acrylate formation was found to be highly sensitive to base strength, with only strongly basic alkoxides (pK_a of 37–40)[55–59] being effective in promoting productive deprotonation. Increasing the loading of NaO^{t}Bu from 1 to 10 or 20 equivalents led to a gradual improvement in acrylate yield, reaching up to 40%, demonstrating that direct deprotonation is a viable pathway for acrylate generation.

Recently, Pasha *et al.* proposed an alternative pathway, in which direct proton transfer from the β-carbon to the carbonyl oxygen is promoted by a Lewis acid/base pair (LiI/NEt$_3$).[60] While this mechanism is viable in the nickel system with relatively weak bases (NEt$_3$, pK_a of 18), analogous Lewis acid/weak base combinations, NaBAr$^F_4$ with amine and phosphazene bases spanning pK_a of 18–34, afforded no detectable acrylate (Table 2, entries 1, 2 and 4). The sharp pK_a threshold for productive reactivity (p$K_a \geq 37$) is therefore more consistent with direct C–H cleavage by a strong external base than with base-assisted enolization.

To evaluate the feasibility of β-hydride elimination and deprotonation pathways, reaction coordinates were calculated for each proposed mechanism (Fig. 7). For the direct β-hydride elimination pathway (Fig. 5A), the titanalactone moiety first undergoes ring opening to locate the β-hydrogen in proximity to the titanium center. This structural reorganization requires Ti–O bond dissociation and is highly endergonic (ΔG = +34.9 kcal mol^{-1}). The subsequent β-hydride elimination step involves an additional barrier of 14.8 kcal mol^{-1}, resulting in an overall barrier of +49.7 kcal mol^{-1} (Fig. 7, Path A). Such a

Table 2 Base screening for deprotonation of **2** to produce acrylate

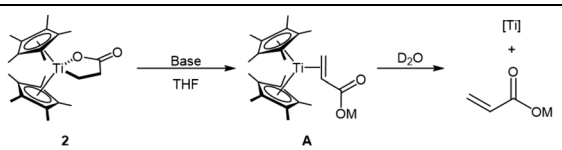

2 **A**

Entry	Base	Additive	pK_a [a]	Yield [b] (%)
1	NEt$_3$	NaBAr$^F_4$	18.8	—
2	DBU	NaBAr$^F_4$	24.3	—
3	NaOPh-2-F	—	25.4	—
4	^{tBu}P$_1$(pyrr)$_3$ [c]	NaBAr$^F_4$	28.4	—
5	Verkade's base[c]	NaBAr$^F_4$	33.6	—
6	NaOMe	—	~37	11
7	NaO^{i}Pr	—	~39	11
8	NaO^{t}Bu (1 equiv.)	—	~40	24
9	NaO^{t}Bu (10 equiv.)	—	~40	39
10	NaO^{t}Bu (20 equiv.)	—	~40	40

[a] pK_a of the conjugate acid in MeCN. Values are taken from ref. 55–59. [b] Yield determined by ^{1}H NMR analysis using 3-(trimethylsilyl)propionic-2,2,3,3-d_4 acid sodium salt as an internal standard. [c] NaBAr$^F_4$ was added as an additive.

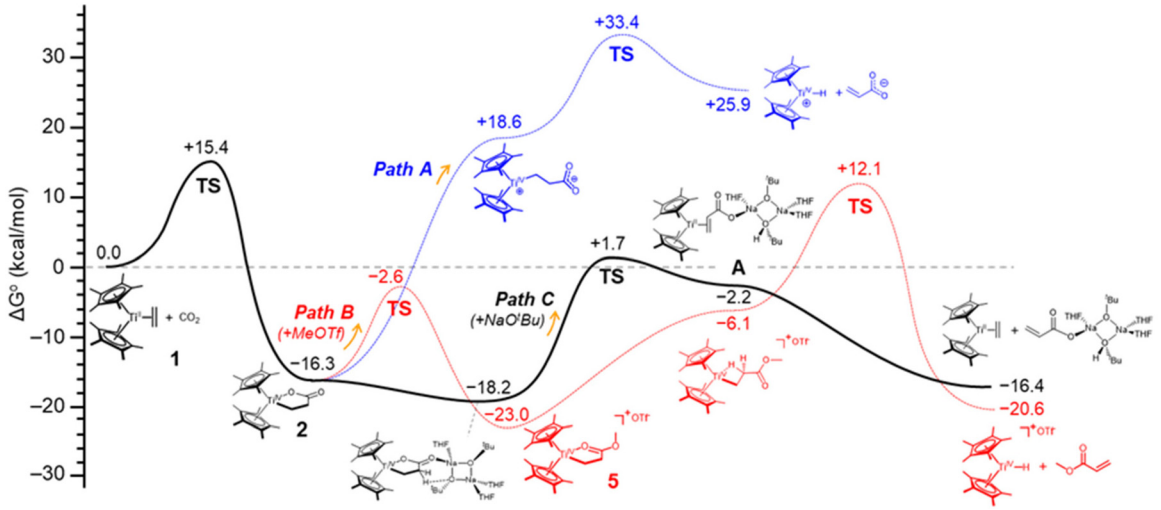

Fig. 7 Calculated free-energy profiles for acrylate formation from CO_2 and ethylene by Cp^*_2Ti *via* direct β-hydride elimination (Path A, blue), MeOTf-promoted β-hydride elimination (Path B, red) and direct deprotonation by NaO^{t}Bu (Path C, black).

prohibitively high barrier strongly indicates that direct β-hydride elimination from **2** is kinetically inaccessible.

Meanwhile, the methylation of **2** with MeOTf is computed to be thermodynamically favorable (ΔG = −6.7 kcal mol^{-1}) and kinetically accessible ($\Delta G^{\ddagger}$ = +13.7 kcal mol^{-1}), consistent with the experimentally observed rapid formation of **5** (Fig. 7, Path B). Methylation weakens the Ti–O bond and enables ring opening to form a *syn*-coplanar Ti–C–C–H arrangement (ΔG = +16.9 kcal mol^{-1}, Fig. 7, Path B). Consequently, β-hydride elimination from **5** leading to methyl acrylate proceeds with a computed activation barrier of +35.1 kcal mol^{-1}, which is substantially lower than that of the non-methylated pathway (Path A, $\Delta G^{\ddagger}$ = +49.7 kcal mol^{-1}). Nevertheless, the overall kinetic barrier remains relatively high, and the thermodynamic driving force of methyl acrylate formation is modest (ΔG = −4.3 kcal mol^{-1}), in good agreement with the experimentally observed sluggish conversion of **5**.

The DFT-computed reaction profile for NaO^{t}Bu-assisted deprotonation of **2** was also calculated (Fig. 7, Path C). Coordination of the distal oxygen atom of the titanalactone to the sodium cation in the NaO^{t}Bu-THF adduct stabilizes intermediate **2** by 1.9 kcal mol^{-1}. The thermodynamics of the subsequent deprotonation step is uphill by 15.2 kcal mol^{-1}, consistent with the experimentally observed untrappability of the putative intermediate **A**. This endergonic step can be driven forward by coupling with the exergonic release of sodium acrylate, accompanied by ethylene coordination (ΔG = −14.2 kcal mol^{-1}). The free-energy profile further indicates that NaO^{t}Bu-assisted deprotonation proceeds with a barrier ($\Delta G^{\ddagger}$ = +19.9 kcal mol^{-1}) higher than that for titanalactone formation ($\Delta G^{\ddagger}$ = +15.4 kcal mol^{-1}) (Fig. 7). This suggests that deprotonation is readily accessible at room temperature but is still slower than the titanalactone formation step. These results are in good agreement with the experimentally observed relative rates of each elementary step. Along Path C, the overall thermodynamics of the catalytic sequence is −16.4 kcal mol^{-1}, supporting the feasibility of the catalytic reaction.

Based on the experimental observations and DFT analysis suggesting that deprotonation of **2** enables the generation of acrylate, we examined whether this pathway could support catalytic turnover. Under mild conditions (25 °C, 1 bar C_2H_4, 5 bar CO_2), catalytic acrylate formation was observed with a TON of 2.1 (Table 3, entry 4). Although this value is far lower than those for reported Ni and Pd catalysts, the observation of any turnover under such mild conditions is mechanistically informative. The Ti center is fundamentally capable of operating catalytically under mild conditions, which is in notable contrast to late transition metal systems.[13–24] Variation of reaction parameters revealed that the limited TON is not dictated by reaction conditions. Neither increasing pressure nor elevating temperature improved performance (Table 3, entries 5–9). This

Table 3 Proof-of-concept catalysis using **2**[a]

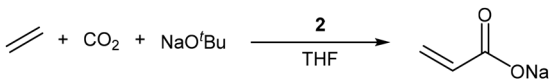

Entry	**2** (mmol)	NaO^{t}Bu (mmol)	$P_{C_2H_4}$ (bar)	P_{CO_2} (bar)	Temp. (°C)	TON[b]
1	0.1	2.0	1	1	25	1.7
2	0	0.2	1	1	25	0
3	0.1	0	1	1	25	0
4	0.1	2.0	1	5	25	2.1
5	0.1	2.0	1	30	25	1.7
6	0.1	2.0	5	5	25	0.5
7	0.1	2.0	30	1	25	0.6
8	0.1	2.0	1	5	80	1.4
9	0.1	2.0	1	5	120	1.2

[a] Standard conditions: NaO^{t}Bu (2.0 mmol), **2** (0.1 mmol), 10 mL THF, 15 h. [b] TON determined by ^{1}H NMR analysis using 3-(trimethylsilyl) propionic-2,2,3,3-d_4 acid sodium salt as an internal standard.

indicates an intrinsic limitation within the Ti system, or a competing process, rather than a simple dependence of kinetics on external parameters.

Mechanistic investigation of the side reaction in the deprotonation of 2

To identify the factor responsible for limiting catalytic turnover, we investigated the reaction of **2** with NaO^{t}Bu. Upon addition of NaO^{t}Bu, compound **2** completely disappeared within 1 h in the ^{1}H NMR spectrum, accompanied by the formation of paramagnetic species, as indicated by magnetic susceptibility measurement using the Evans method.[61] For clear observation and the characterization of the paramagnetic species, the reaction was monitored with EPR spectroscopy. The EPR study at 298 K revealed two distinct signals at g_{iso} = 1.983 and 1.978 that grew over the course of the reaction (Fig. 8A). The significant deviation of the g_{iso} value from 2.0023 indicates titanium-centered paramagnetic species. Consistent with this assignment, UV-Vis monitoring also showed d–d transitions at 615 nm (ε = 39 M^{-1} cm^{-1}) and 779 nm (ε = 35 M^{-1} cm^{-1}) (Fig. 8B).

We assumed that two paramagnetic species arise from a redox process involving the Ti^{IV}-lactone (**2**) and the Ti^{II}-acrylate species **A** generated upon deprotonation of **2** (Fig. 8C). To test this hypothesis, we independently synthesized the Ti^{III}-lactone [Na(THF)$_2$][Cp*$_2$Ti(C$_2$H$_4$CO$_2$)] (**6**) and the Ti^{III}-acrylate Cp*$_2$Ti(O$_2$CCH=CH$_2$) (**7**) (Fig. 9A and B). Compound **6** was prepared by reducing **2** with sodium naphthalenide, while **7** was prepared by salt metathesis of Cp*$_2$Ti(OTf)[62] with tetrabutylammonium acrylate. The EPR spectra of **6** and **7** show signals at g = 1.983 and 1.977, respectively, matching those observed during the deprotonation of **2** with NaO^{t}Bu (Fig. 8A). The UV-Vis spectra of **6** and **7** also reproduce the d–d bands observed in the reaction mixture (Fig. 8B). Furthermore, the reaction mixture spectrum is well described by the sum of the authentic spectra of **6** and **7** in a 1 : 1 ratio, indicating quantitative (>98%) formation of these two species relative to the initial titanium. This suggests that **A** undergoes rapid comproportionation with **2** immediately upon its formation (**2** + **A** → **6** + **7**), preventing its accumulation. Low-temperature UV-Vis monitoring of the reaction (−40 to 0 °C) showed only the formation of **6** and **7**, with no other detectable intermediates (Fig. S31).

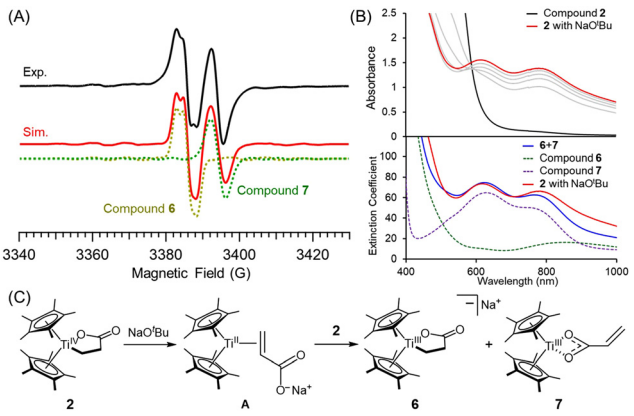

Fig. 8 (A) EPR spectrum of the reaction mixture of **2** with NaO^{t}Bu (10 equiv.) in THF with simulated contributions from **6** and **7**. (B) UV-Vis spectral changes during the reaction of **2** with 10 equiv. of NaO^{t}Bu over 1 h (top), and the corresponding extinction coefficients of the reaction mixture compared with those of **6** and **7**. (C) Generation of **6** and **7** *via* comproportionation of **2** with the Ti^{II}-acrylate species **A**.

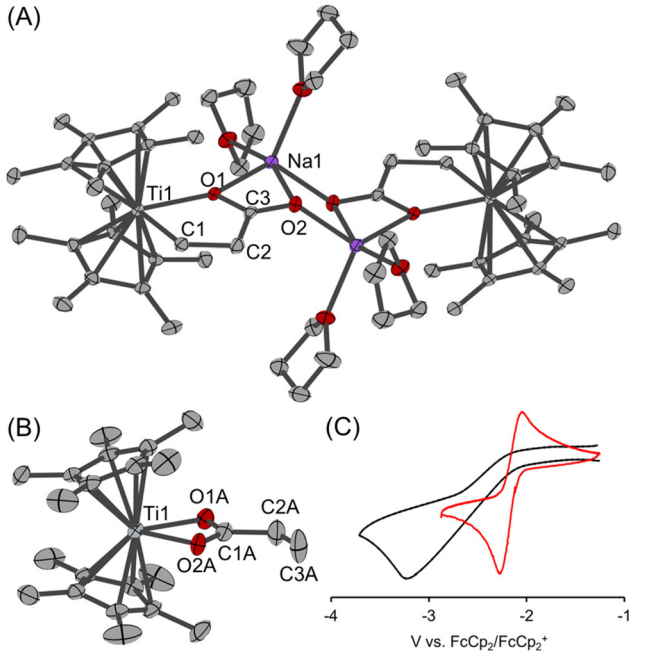

Fig. 9 (A) Solid-state structure of **6**, (B) solid-state structure of **7**, (C) cyclic voltammograms of **2** (red) and **7** (black).

The driving force of the proposed comproportionation reaction was evaluated by electrochemical analysis. The cyclic voltammogram shows a reversible Ti$^{III/IV}$ couple for **2** at an $E_{1/2}$ of −2.15 V and an irreversible Ti$^{II/III}$ couple for **7** at an E_{pc} of −3.23 V *vs.* Fc/Fc$^+$ (Fig. 9C), corresponding to favorable thermodynamics (ΔG = −24.9 kcal mol^{-1}) for comproportionation between **2** and **A** to form **6** and **7**. In addition, a potential alternative pathway involving single-electron transfer (SET) from NaO^{t}Bu to **2** is implausible due to the far more negative Ti$^{III/IV}$ couple (−2.15 V) compared to the ^{t}BuO$^\bullet$/^{t}BuO$^-$ couple (−0.4 V *vs.* Fc/Fc$^+$).[63] Furthermore, acrylate formation does not proceed when the Ti^{III} species **6** is treated with NaO^{t}Bu.

Complexes **6** and **7** were detected not only under stoichiometric deprotonation conditions but also in reaction mixtures obtained after catalytic acrylate formation. This observation indicates that comproportionation is not merely a pathway under stoichiometric conditions, but also an operative process under the catalytic conditions. While the accumulation of **6** and **7** suggests that these species constitute the dominant titanium reservoirs after turnover, they are best regarded as off-cycle species formed through a thermodynamically favoured redox equilibrium rather than as productive resting states of the catalytic cycle.

Accordingly, we investigated the effect of external oxidants on reoxidization of Ti^{III}-lactone (**6**) to Ti^{IV} (**2**) (Table 4). In the absence of an oxidant, the yield was limited to 39%. The use of $[Cp_2Co][PF_6]$ ($E_{1/2}$ = −1.33 V)[64] resulted in a significant increase in acrylate yield under stoichiometric deprotonation conditions (Table 4, entries 2–5). Increasing the amount of $[Cp_2Co][PF_6]$ up to 0.5 equiv. led to a gradual enhancement of acrylate formation, reaching 72%. Further addition beyond 0.5 equiv. did not improve the outcome, consistent with the generation of 0.5 equiv. of **6** *via* comproportionation. In contrast, stronger oxidants, such as $[C_7H_7][BF_4]$ and AgOTf, did not improve acrylate formation. These oxidants likely engage in competing chemical or redox interactions with NaO^{t}Bu or other Ti species rather than reoxidizing **6**. Thus, careful selection of a suitable oxidant capable of selectively oxidizing Ti^{III} without interfering with other components of the reaction mixture is essential for productive acrylate formation.

Although this oxidant effect is clear under stoichiometric conditions, catalytic attempts with $[Cp_2Co][PF_6]$ afforded a TON of 2.0, showing no improvement over base-only conditions. Control experiments indicate that $[Cp_2Co][PF_6]$ reacts readily with both NaO^{t}Bu and **1** (Fig. S30), suggesting that the oxidant would be intercepted by the alkoxide base and Ti(II) species rather than productively reoxidizing **6**. Despite these limitations, the oxidation experiment demonstrates that suppressing the accumulation of Ti(III) species enables acrylate formation in high yield.

The observations described above can be rationalized by the mechanistic picture summarized in Fig. 10. Deprotonation of the titanalactone (**2**) generates the reduced intermediate **A**, which can proceed along the productive pathway to release acrylate and regenerate **1** or be diverted into a thermodynamically favored off-cycle sink *via* comproportionation to form **6** and **7** (Fig. 10). This thermodynamic stabilization accounts for the accumulation of Ti^{III} species and the resulting suppression of turnover.

Table 4 Additive effect for deprotonation of **2** to produce acrylate[a]

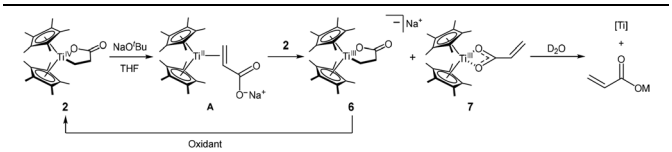

Entry	Additive	Equivalent[a]	$E_{1/2}$ (*vs.* Fc/Fc$^+$)[52]	Yield[b] (%)
1	—	—	—	39
2	$[Cp_2Co][PF_6]$	0.1	−1.33	53
3	$[Cp_2Co][PF_6]$	0.25	−1.33	64
4	$[Cp_2Co][PF_6]$	0.5	−1.33	72
5	$[Cp_2Co][PF_6]$	1	−1.33	72
6	$[C_7H_7][BF_4]$	1	−0.65	15
7	AgOTf	1	+0.18	25

[a] Amount of oxidant relative to compound **2**. [b] Yield determined by ^{1}H NMR analysis using 3-(trimethylsilyl)propionic-2,2,3,3-d_4 acid sodium salt as an internal standard.

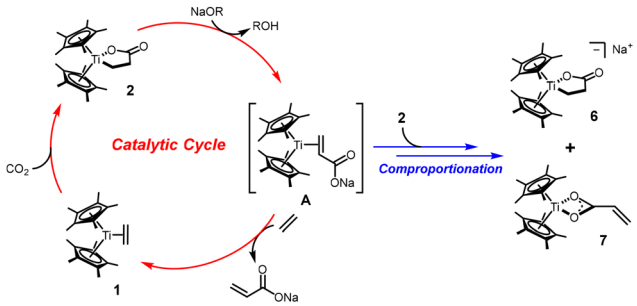

Fig. 10 Mechanistic overview highlighting catalytic and off-cycle pathways.

Conclusions

This study establishes a mechanistic understanding of CO_2/ethylene coupling mediated by titanium complexes. Kinetic and thermodynamic analyses reveal that titanalactone formation is both rapid and exergonic, demonstrating inherent advantages of titanium over late transition metals. The strong Ti–O interaction stabilizes the titanalactone intermediate but inhibits subsequent β-hydride elimination. Instead, deprotonation with alkoxide bases provides a viable alternative pathway. A proof-of-concept catalytic experiment under mild conditions supports this mechanistic picture.

Notably, we identified comproportionation between Ti^{II} and Ti^{IV} intermediates as a key off-cycle pathway that limits turnover, which has not been recognized in previous carboxylation systems. Rather than elementary steps, redox compatibility across the catalytic intermediates therefore emerges as a key challenge in titanium-based carboxylation catalysis. Although reoxidation restores high-yield acrylate formation under stoichiometric conditions, achieving efficient catalytic turnover will require an oxidant or redox strategy compatible with the full set of catalytic intermediates. These findings define both the opportunities and the current mechanistic constraints of titanium-mediated CO_2/ethylene coupling and provide a basis for the future development of early transition metal systems for carboxylation chemistry.

Author contributions

C. Y. designed and supervised the project. A. K., N. S. and M. L. designed, conducted, and analysed the results of experiments. Y. K. H assisted with the high-pressure reactions and contributed to early discussions of the project. J. S. performed and analysed the EPR and computational studies and contributed to discussion of the project. C. Y., J. S., and A. K. wrote the manuscript with input from all coauthors.

Conflicts of interest

There are no conflicts to declare.

Data availability

All data supporting the findings of this study are available within the article and its supplementary information (SI). Supplementary information: characterization data (NMR, EPR, UV–Vis, IR, CV and crystallography), kinetic data, and computational details. See DOI: **https://doi.org/10.1039/d6qi00548a**.

CCDC 2463344–2463347 (for **2**, **5**, **6** and **7**) contain the supplementary crystallographic data for this paper.[65a–d]

Acknowledgements

This research was supported by the National Research Foundation of Korea (RS-2025-00514821, RS-2022-NR068725, RS-2025-02215028) and the Settlement Research Fund of UNIST (Ulsan National Institute of Science & Technology). We thank the UNIST Office of Research Facilities and Training (ResFacT) for support in using the equipment. The EPR measurements were supported by the Institute for Basic Science (IBS-R010-D1) in Korea. Experiments at PLS-II were supported in part by MSIT and POSTECH.

References

1 S. Dabral and T. Schaub, The Use of Carbon Dioxide (CO_2) as a Building Block in Organic Synthesis from an Industrial Perspective, *Adv. Synth. Catal.*, 2019, **361**, 223–246.
2 M. D. Burkart, N. Hazari, C. L. Tway and E. L. Zeitler, Opportunities and Challenges for Catalysis in Carbon Dioxide Utilization, *ACS Catal.*, 2019, **9**, 7937–7956.
3 A. Tortajada, F. Juliá-Hernández, M. Börjesson, T. Moragas and R. Martin, Transition–Metal–Catalyzed Carboxylation Reactions with Carbon Dioxide, *Angew. Chem., Int. Ed.*, 2018, **57**, 15948–15982.
4 Q. Liu, L. Wu, R. Jackstell and M. Beller, Using carbon dioxide as a building block in organic synthesis, *Nat. Commun.*, 2015, **6**, 5933.
5 T. Fujihara, in *Chemical Valorisation of Carbon Dioxide*, ed. G. Stefanidis and A. Stankiewicz, The Royal Society of Chemistry, 2022, pp. 19–61.
6 R. Cauwenbergh, V. Goyal, R. Maiti, K. Natte and S. Das, Challenges and recent advancements in the transformation of CO_2 into carboxylic acids: straightforward assembly with homogeneous 3d metals, *Chem. Soc. Rev.*, 2022, **51**, 9371–9423.
7 J. Davies, J. R. Lyonnet, D. P. Zimin and R. Martin, The road to industrialization of fine chemical carboxylation reactions, *Chem*, 2021, **7**, 2927–2942.
8 T. Ohara, T. Sato, N. Shimizu, G. Prescher, H. Schwind, O. Weiberg, K. Marten, H. Greim, T. D. Shaffer and P. Nandi, in *Ullmann's Encyclopedia of Industrial Chemistry*, Wiley–VCH Verlag GmbH & Co. KGaA, Wiley, 1st edn, 2020, pp. 1–21.
9 T. Schaub, in *Organometallics in Process Chemistry*, ed. T. J. Colacot and V. Sivakumar, Springer International Publishing, Cham, 2018, vol. 65, pp. 253–270.
10 X. Wang, H. Wang and Y. Sun, Synthesis of Acrylic Acid Derivatives from CO_2 and Ethylene, *Chem*, 2017, **3**, 211–228.
11 N. Y. Kuznetsov, A. L. Maximov and I. P. Beletskaya, Synthesis of acrylic acid and acrylates from CO_2 and ethylene—the thorny path from dream to reality, *Russ. Chem. Rev.*, 2024, **93**, RCR5147.
12 N. Maity, N. Garcia, E. A. Jaseer, S. Barman, A. M. Aitani, M. M. Tijani and N. Al-Yassir, Advancement of catalyst systems towards the formation of acrylates from CO2 and ethylene, *Renewable Sustainable Energy Rev.*, 2024, **200**, 114483.
13 M. L. Lejkowski, R. Lindner, T. Kageyama, G. É. Bódizs, P. N. Plessow, I. B. Müller, A. Schäfer, F. Rominger, P. Hofmann, C. Futter, S. A. Schunk and M. Limbach, The First Catalytic Synthesis of an Acrylate from CO_2 and an Alkene-A Rational Approach, *Chem. – Eur. J.*, 2012, **18**, 14017–14025.
14 C. Hendriksen, E. A. Pidko, G. Yang, B. Schäffner and D. Vogt, Catalytic Formation of Acrylate from Carbon Dioxide and Ethene, *Chem. – Eur. J.*, 2014, **20**, 12037–12040.
15 N. Huguet, I. Jevtovikj, A. Gordillo, M. L. Lejkowski, R. Lindner, M. Bru, A. Y. Khalimon, F. Rominger, S. A. Schunk, P. Hofmann and M. Limbach, Nickel-Catalyzed Direct Carboxylation of Olefins with CO_2 : One-Pot Synthesis of α,β-Unsaturated Carboxylic Acid Salts, *Chem. – Eur. J.*, 2014, **20**, 16858–16862.
16 S. Manzini, N. Huguet, O. Trapp and T. Schaub, Palladium- and Nickel-Catalyzed Synthesis of Sodium Acrylate from Ethylene, CO_2, and Phenolate Bases: Optimization of the Catalytic System for a Potential Process: Pd- and Ni-Catalyzed Synthesis of Sodium Acrylate, *Eur. J. Org. Chem.*, 2015, 7122–7130.
17 S. C. E. Stieber, N. Huguet, T. Kageyama, I. Jevtovikj, P. Ariyananda, A. Gordillo, S. A. Schunk, F. Rominger, P. Hofmann and M. Limbach, Acrylate formation from CO_2 and ethylene: catalysis with palladium and mechanistic insight, *Chem. Commun.*, 2015, **51**, 10907–10909.
18 I. Knopf, D. Tofan, D. Beetstra, A. Al-Nezari, K. Al-Bahily and C. C. Cummins, A family of cis-macrocyclic diphosphines: modular, stereoselective synthesis and application in catalytic CO_2/ethylene coupling, *Chem. Sci.*, 2017, **8**, 1463–1468.
19 S. Manzini, N. Huguet, O. Trapp, R. A. Paciello and T. Schaub, Synthesis of acrylates from olefins and CO2 using sodium alkoxides as bases, *Catal. Today*, 2017, **281**, 379–386.
20 S. Manzini, A. Cadu, A.-C. Schmidt, N. Huguet, O. Trapp, R. Paciello and T. Schaub, Enhanced Activity and Recyclability of Palladium Complexes in the Catalytic Synthesis of Sodium Acrylate from Carbon Dioxide and Ethylene, *ChemCatChem*, 2017, **9**, 2269–2274.

21 M. N. Hopkins, K. Shimmei, K. B. Uttley and W. H. Bernskoetter, Synthesis and Reactivity of 1,2-Bis(di-*iso*-propylphosphino)benzene Nickel Complexes: A Study of Catalytic CO_2 –Ethylene Coupling, *Organometallics*, 2018, **37**, 3573–3580.

22 K. Takahashi, K. Cho, A. Iwai, T. Ito and N. Iwasawa, Development of *N*–Phosphinomethyl–Substituted NHC–Nickel(0) Complexes as Robust Catalysts for Acrylate Salt Synthesis from Ethylene and CO_2, *Chem. – Eur. J.*, 2019, **25**, 13504–13508.

23 K. B. Uttley, K. Shimmei and W. H. Bernskoetter, Ancillary Ligand and Base Influences on Nickel-Catalyzed Coupling of CO_2 and Ethylene to Acrylate, *Organometallics*, 2020, **39**, 1573–1579.

24 C. Kang, S. Kim, W. Han, H. Ryu, W. Seong, J. Kim, D.-A. Park, S. Park, K. Park, H. M. Park, H. T. Kim, C. H. Lee and S. Hong, In situ generated diphenylphosphine-chelated imidazo[1,5-a]pyridin-3-ylidene nickel (0) catalysts for highly efficient acrylate synthesis from ethylene and CO2, *J. CO2 Util.*, 2025, **91**, 103004.

25 K. Y. Kunihiro, A. Marty, L. Chahen, L. Magna and J. M. Asensio, Sodium Acrylate Synthesis Through CO_2 and Ethylene Coupling Catalyzed by Pd: Solvent Effects and $PdBr_2$ as a Surprisingly Suitable Precursor, *ChemCatChem*, 2024, **16**, e202401074.

26 I. Knopf, M.-A. Courtemanche and C. C. Cummins, Cobalt Complexes Supported by *cis* -Macrocyclic Diphosphines: Synthesis, Reactivity, and Activity toward Coupling Carbon Dioxide and Ethylene, *Organometallics*, 2017, **36**, 4834–4843.

27 T. Ito, K. Takahashi and N. Iwasawa, Reactivity of a Ruthenium(0) Complex Bearing a Tetradentate Phosphine Ligand: Applications to Catalytic Acrylate Salt Synthesis from Ethylene and CO_2, *Organometallics*, 2019, **38**, 205–209.

28 K. Takahashi, Y. Hirataka, T. Ito and N. Iwasawa, Mechanistic Investigations of the Ruthenium-Catalyzed Synthesis of Acrylate Salt from Ethylene and CO_2, *Organometallics*, 2020, **39**, 1561–1572.

29 S. Takegasa, M. M. Lee, K. Tokuhiro, R. Nakano and M. Yamashita, Rhodium–Catalyzed Acrylate Synthesis from Carbon Dioxide and Ethylene by using a Guanidine–Based Pincer Ligand: Perturbing Occupied d–Orbitals by pπ–dπ Repulsion Makes a Difference, *Chem. – Eur. J.*, 2022, **28**, e202201870.

30 T. T. Adamson, L. G. Reeder, S. P. Kelley and W. H. Bernskoetter, Zerovalent Triphosphine Ruthenium Complexes for Coupling Carbon Dioxide and Ethylene, *Organometallics*, 2025, **44**, 385–393.

31 K. Kunihiro, T. Rajeshkumar, L. Maron, S. Heyte, S. Paul, T. Roisnel, J.-F. Carpentier and E. Kirillov, On the Mechanism of Acrylate and Propionate Silyl Esters Synthesis by Ruthenium-Catalyzed Coupling of CO2 with C2H4 in the Presence of Hydrosilanes: Combined Experimental and Computational Investigations, *Mol. Catal.*, 2025, **570**, 114660.

32 S. M. Rummelt, H. Zhong, I. Korobkov and P. J. Chirik, Iron-Mediated Coupling of Carbon Dioxide and Ethylene: Macrocyclic Metallalactones Enable Access to Various Carboxylates, *J. Am. Chem. Soc.*, 2018, **140**, 11589–11593.

33 Y. Li, Z. Liu, R. Cheng and B. Liu, Mechanistic Aspects of Acrylic Acid Formation from CO_2-Ethylene Coupling over Palladium- and Nickel-based Catalysts, *ChemCatChem*, 2018, **10**, 1420–1430.

34 P. N. Plessow, A. Schäfer, M. Limbach and P. Hofmann, Acrylate Formation from CO_2 and Ethylene Mediated by Nickel Complexes: A Theoretical Study, *Organometallics*, 2014, **33**, 3657–3668.

35 Y. Zhu, Y. Mu, H. Shen, L. Sun, Z. Zeng and Z. Liu, The formation of nickelalactone in CO2/C2H4 coupling reaction: A benchmark, dispersion correction, and energy decomposition analysis, *Mol. Catal.*, 2024, **558**, 113996.

36 S. A. Cohen and J. E. Bercaw, Titanacycles derived from reductive coupling of nitriles, alkynes, acetaldehyde, and carbon dioxide with bis(pentamethylcyclopentadienyl)(ethylene)titanium(II), *Organometallics*, 1985, **4**, 1006–1014.

37 B. Hessen, A. Meetsma and J. H. Teuben, An ethylene complex of vanadium: synthesis, structure, and reactivity of cyclopentadienylbis(trimethylphosphine)(ethylene) vanadium(I), *J. Am. Chem. Soc.*, 1988, **110**, 4860–4861.

38 H. G. Alt and C. E. Denner, Metallacyclen des zirkonocens, *J. Organomet. Chem.*, 1990, **390**, 53–60.

39 R. Alvarez, E. Carmona, D. J. Cole-Hamilton, A. Galindo, E. Gutierrez-Puebla, A. Monge, M. L. Poveda and C. Ruiz, Formation of acrylic acid derivatives from the reaction of carbon dioxide with ethylene complexes of molybdenum and tungsten, *J. Am. Chem. Soc.*, 1985, **107**, 5529–5531.

40 A. Galindo, A. Pastor, P. J. Perez and E. Carmona, Bis(ethylene) complexes of molybdenum and tungsten and their reactivity toward carbon dioxide. New examples of acrylate formation by coupling of ethylene and carbon dioxide, *Organometallics*, 1993, **12**, 4443–4451.

41 W. H. Bernskoetter and B. T. Tyler, Kinetics and Mechanism of Molybdenum-Mediated Acrylate Formation from Carbon Dioxide and Ethylene, *Organometallics*, 2011, **30**, 520–527.

42 J. M. Wolfe and W. H. Bernskoetter, Reductive functionalization of carbon dioxide to methyl acrylate at zerovalent tungsten, *Dalton Trans.*, 2012, **41**, 10763.

43 I. A. Tonks, Ti-Catalyzed and -Mediated Oxidative Amination Reactions, *Acc. Chem. Res.*, 2021, **54**, 3476–3490.

44 M. Manßen and L. L. Schafer, Titanium catalysis for the synthesis of fine chemicals – development and trends, *Chem. Soc. Rev.*, 2020, **49**, 6947–6994.

45 Z. W. Davis-Gilbert and I. A. Tonks, Titanium redox catalysis: insights and applications of an earth-abundant base metal, *Dalton Trans.*, 2017, **46**, 11522–11528.

46 E. P. Beaumier, A. J. Pearce, X. Y. See and I. A. Tonks, Modern applications of low-valent early transition metals in synthesis and catalysis, *Nat. Rev. Chem.*, 2018, **3**, 15–34.

47 J. Pinkas, I. Císařová, R. Gyepes, J. Kubišta, M. Horáček and K. Mach, Ethene Complexes of Bulky Titanocenes,

Their Thermolysis, and Their Reactivity toward 2-Butyne, *Organometallics*, 2012, **31**, 5478–5493.

48 S. A. Cohen, P. R. Auburn and J. E. Bercaw, Structure and reactivity of bis(pentamethylcyclopentadienyl)(ethylene) titanium(II), a simple olefin adduct of titanium, *J. Am. Chem. Soc.*, 1983, **105**, 1136–1143.

49 Y. Li, Z. Liu, J. Zhang, R. Cheng and B. Liu, Insights into the Base–Assisted Acrylate Formation from CO_2 /C_2 H_4 Coupling by Pd– and Ni–catalyst: A DFT Mechanistic Study, *ChemCatChem*, 2018, **10**, 5669–5678.

50 S. Y. T. Lee, M. Cokoja, M. Drees, Y. Li, J. Mink, W. A. Herrmann and F. E. Kühn, Transformation of Nickelalactones to Methyl Acrylate: On the Way to a Catalytic Conversion of Carbon Dioxide, *ChemSusChem*, 2011, **4**, 1275–1279.

51 C. Bruckmeier, M. W. Lehenmeier, R. Reichardt, S. Vagin and B. Rieger, Formation of Methyl Acrylate from CO_2 and Ethylene via Methylation of Nickelalactones, *Organometallics*, 2010, **29**, 2199–2202.

52 S. Y. T. Lee, A. A. Ghani, V. D'Elia, M. Cokoja, W. A. Herrmann, J.-M. Basset and F. E. Kühn, Liberation of methyl acrylate from metallalactone complexes via M–O ring opening (M = Ni, Pd) with methylation agents, *New J. Chem.*, 2013, **37**, 3512.

53 P. N. Plessow, L. Weigel, R. Lindner, A. Schäfer, F. Rominger, M. Limbach and P. Hofmann, Mechanistic Details of the Nickel-Mediated Formation of Acrylates from CO_2, Ethylene and Methyl Iodide, *Organometallics*, 2013, **32**, 3327–3338.

54 Z. Zhang, F. Guo, F. E. Kühn, J. Sun, M. Zhou and X. Fang, Liberation of acrylates from nickelalactones via Ni—O ring opening with alkyl iodides: The Ni-O ring opening of nickelalactones using alkyl iodides, *Appl. Organomet. Chem.*, 2017, **31**, e3567.

55 C. R. Waidmann, A. J. M. Miller, C.-W. A. Ng, M. L. Scheuermann, T. R. Porter, T. A. Tronic and J. M. Mayer, Using combinations of oxidants and bases as PCET reactants: thermochemical and practical considerations, *Energy Environ. Sci.*, 2012, **5**, 7771.

56 M. Penhoat, Scope and limitations of a ^{1}H NMR method for the prediction of substituted phenols pKa values in water, CH_3CN, DMF, DMSO and i-PrOH, *Tetrahedron Lett.*, 2013, **54**, 2571–2574.

57 S. Tshepelevitsh, A. Kütt, M. Lõkov, I. Kaljurand, J. Saame, A. Heering, P. G. Plieger, R. Vianello and I. Leito, On the Basicity of Organic Bases in Different Media, *Eur. J. Org. Chem.*, 2019, 6735–6748.

58 P. B. Kisanga, J. G. Verkade and R. Schwesinger, p K_a Measurements of P(RNCH$_2$CH$_3$)$_3$N, *J. Org. Chem.*, 2000, **65**, 5431–5432.

59 W. N. Olmstead, Z. Margolin and F. G. Bordwell, Acidities of water and simple alcohols in dimethyl sulfoxide solution, *J. Org. Chem.*, 1980, **45**, 3295–3299.

60 F. A. Pasha, D. Beetstra, M. Al-Ghamdi and K. AlBahily, Novel Insight for Acrylate Formation Using CO2 /Ethylene Coupling, *Eur. J. Inorg. Chem.*, 2025, **28**, e202500168.

61 D. F. Evans, 400. The determination of the paramagnetic susceptibility of substances in solution by nuclear magnetic resonance, *J. Chem. Soc.*, 1959, 2003.

62 M. Kessler, S. Hansen, D. Hollmann, M. Klahn, T. Beweries, A. Spannenberg, A. Brückner and U. Rosenthal, Synthesis of Cp*$_2$ Ti(OTf) and Its Reaction with Water, *Eur. J. Inorg. Chem.*, 2011, **2011**, 627–631.

63 J. P. Barham, G. Coulthard, K. J. Emery, E. Doni, F. Cumine, G. Nocera, M. P. John, L. E. A. Berlouis, T. McGuire, T. Tuttle and J. A. Murphy, KO*t*Bu: A Privileged Reagent for Electron Transfer Reactions?, *J. Am. Chem. Soc.*, 2016, **138**, 7402–7410.

64 N. G. Connelly and W. E. Geiger, Chemical Redox Agents for Organometallic Chemistry, *Chem. Rev.*, 1996, **96**, 877–910.

65 (*a*) CCDC 2463344: Experimental Crystal Structure Determination, 2026, DOI: **10.5517/ccdc.csd.cc2np9qd**; (*b*) CCDC 2463345: Experimental Crystal Structure Determination, 2026, DOI: **10.5517/ccdc.csd.cc2np9rf**; (*c*) CCDC 2463346: Experimental Crystal Structure Determination, 2026, DOI: **10.5517/ccdc.csd.cc2np9sg**; (*d*) CCDC 2463347: Experimental Crystal Structure Determination, 2026, DOI: **10.5517/ccdc.csd.cc2np9th**.